Detection and direction discrimination of single vortex rings by harbour seals (*Phoca vitulina*)

Yvonne Krüger, Wolf Hanke, Lars Miersch, Guido Dehnhardt

University of Rostock, Institute for Biosciences, Sensory and Cognitive Ecology, Albert-Einstein-Straße 3, Rostock 18059, Germany

Corresponding author's email address

yvonne.krueger@uni-rostock.de

Keywords

Vibrissae

Hydrodynamic sensory system

Vortex ring

Pinnipeds

Harbour seal

SUMMARY STATEMENT

Harbour seals are able to detect a variety of different vortex rings and are capable of analysing the travel direction of a single vortex ring perceived by the mystacial vibrissae.

ABSTRACT

Harbour seals possess highly sensitive vibrissae that enable them to track hydrodynamic trails left behind by a swimming fish. Most of these trails contain vortex rings as a main hydrodynamic component. They may reveal information about their generator as the trails differ depending on the fish species, the fish's body shape, size, and swimming style. Additionally, fish generate single vortex rings in diverse natural situations. In this study, the ability of blindfolded stationary harbour seals to detect and analyse single vortex rings regarding directional information has been investigated. In three different behavioural experiments, the animals were trained to respond to single artificially generated vortex rings. The results show that harbour seals are able to respond to a variety of different vortex rings upon vibrissal stimulation. The investigation of the minimum hydrodynamically perceivable angle revealed that it is at least as small as 5.7°, which was the smallest adjustable angle. Moreover, harbour seals are capable of analysing the travel direction of a vortex ring perceived by the mystacial pads irrespective of whether the vibrissae were stimulated ipsilaterally or contralaterally. In situations in which no complex hydrodynamic trail is available, it is advantageous for a hunting seal to be able to extract information from a single vortex ring.

INTRODUCTION

All pinnipeds possess well-developed vibrissae (Ling, 1966; Stephens et al., 1973; Dykes, 1975; Ling, 1977). This sensory specialisation enables the perception of haptic information (Kastelein and van Gaalen, 1988; Dehnhardt and Dücker, 1996; Dehnhardt and Kaminski, 1995; Dehnhardt et al., 1998a; Grant et al., 2013), which might be used by pinnipeds for finding benthic prey when actively touching the sea floor. In addition to the haptic function, the vibrissae of harbour seals and California sea lions function as a hydrodynamic receptor system (Dehnhardt et al., 1998b; Dehnhardt and Mauck, 2008), which is well suited to perceive the water disturbances in the wake of a swimming fish. Even several minutes after a fish has disappeared,

these hydrodynamic stimuli can contain water particle velocities significantly higher than background noise (Hanke et al., 2000; Hanke and Bleckmann, 2004) and well above the detection threshold of a harbour seal's vibrissal system (Dehnhardt et al., 1998b). As these fish-generated wakes decay slowly, they can serve as trackable hydrodynamic trails. Diverse studies on different fish species have shown that fish hydrodynamic trails consist of a complex, three-dimensional chain of vortex rings with a median, rearward jet flow undulating between the counter-rotating vortices (Bleckmann et al., 1991; Blickhan et al., 1992; Müller et al., 1997; Videler et al., 1999; Nauen and Lauder, 2002; Lauder and Drucker, 2002).

The structure and spatial arrangement of the vortices as well as the water velocities in these fish trails depend on the fish species, its body shape and size, and the fish's swimming style and speed (Bleckmann et al., 1991; Hanke et al., 2000; Müller et al., 2000; Hanke and Bleckmann, 2004; Standen and Lauder, 2007). Thus, a hydrodynamic trail might provide a predator with relevant information about its generator, e.g. which species it is, its body shape, and size. Moreover, the trail contains directional information about the moving fish, which can be disclosed both by analysing the velocity gradient within the trail and the overall moving direction of the complete water flow. Due to the specific ageing of the trail (decay of vorticity in the vortex street and of flow velocity), it is possible to gain information about how long ago the fish had passed the location at which the seal detected the trail.

Blindfolded harbour seals (Dehnhardt et al., 2001; Schulte-Pelkum et al. 2007; Wieskotten et al., 2010a) and California sea lions (Gläser et al., 2011) are able to detect and precisely follow hydrodynamic trails by means of their mystacial vibrissae and thus locate distant objects. Harbour seals also can discriminate hydrodynamic trails generated by differently sized objects as well as by objects differing in shape (Wieskotten et al., 2011). Moreover, harbour seals are capable of detecting the moving direction of a small artificial fish tail even after the wake had aged for up to 35 s (Wieskotten et al., 2010b). Simultaneous analysis of the hydrodynamic parameters by particle image velocimetry (PIV) during the experiment of Wieskotten et al. (2010b) led to the hypothesis that among all hydrodynamic parameters inherent to a hydrodynamic trail, vortex rings were the relevant structures used by the harbour seal to determine the moving direction of the generator.

Besides the complex chains of linked vortex rings found in some fish wakes (annular seabream (*Diplodus annularis*), Aleyev; 1977; rainbow trout (*Oncorhynchus mykiss*), Blickhan et al., 1992; thick-lipped mullet (*Chelon labrosus* Risso), Müller et al., 1997), it has been shown for several fish species (zebra danio (*Brachydanio albolineatus*), Rosen, 1959; Kuhli loach (*Acanthophthalmus kuhlii*), Rayner, 1995; European eel (*Anguilla Anguilla*), Müller et al., 2001) that also single vortex rings occur in their trails.

Another example of single vortex ring generation is the escape response of a fish (Tytell and Lauder, 2008; Niesterok and Hanke, 2013). During a C-start, rainbow trout generate three clearly distinguishable jets and at least one of these is described as a vortex ring (Niesterok and Hanke, 2013). Moreover, the flow pattern generated by escaping fish provides an aquatic predator with the information required to localise the prey.

As vortex rings have been hypothesised by Wieskotten et al. (2010b) to be crucial for a seal's determination of the directional information inherent in a complex trail, we tested whether harbour seals are able to perceive single vortex rings with their mystacial vibrissae. For this purpose, a variety of reproducible vortex rings differing in size, maximum velocity, and travel velocity were created on the basis of the parameters found in vortex rings characterising natural fish wakes. Besides the ability to detect these artificially generated vortex rings, the main objective of this study was to investigate if harbour seals are able to determine the direction in which a single vortex ring is travelling. Thus, first the determination of the minimum hydrodynamically perceivable angle (MHPA), that is the minimum difference in angle at which the travel direction of a bilaterally perceived single vortex ring is still discernible (compare minimum audible angle, MAA, in Bodson et al., 2007), was approached. Second, the ability of harbour seals to discriminate the travel direction of a vortex ring independent of its travel path through the vibrissal pad (contralateral and ipsilateral), was investigated. This included both bilateral and unilateral (one vibrissal pad only) stimulation. The results of these behavioural experiments give further insight into the sensory capabilities of the pinniped vibrissal system and detail what information a harbour seal can derive from single vortex rings.

MATERIALS AND METHODS

Vortex ring generator

Single vortex rings were produced via two custom-made vortex ring generators (VRGs), constructed from acrylic glass (Fig. 1A). Each VRG consisted of a cube (20 x 20 x 20 cm) with an opening of 6.5 cm in diameter. This opening was covered by attachable blends with a circular aperture of 2 cm in diameter. On the top side, the cube opened to a vertical pipe (inner diameter: 10 cm). A plunger, driven by a remote controlled linear motor (LinMot, NTI AG, Dresden, Germany), was mounted inside the pipe. By pushing down the plunger, water was expelled through the aperture of the blend, thus generating a single vortex ring.

Using the software LinMot-Talk1100, we modified four parameters of the motor configurations, specifically the “amplitude” of the plunger displacement and thus the amount of water that would be expelled, the “acceleration” and “deceleration” of the plunger movement, and its “velocity” (see Tab. 1). By these means, 10 different vortex rings with predefined sizes, maximum flow velocities, and travel velocities similar to those found in fish wakes were produced.

Vortex ring characterisation with Particle Image Velocimetry

Setup and vector field calculation

Flow fields of the vortex rings were visualised by two-dimensional PIV (Adrian, 1991; Willert and Gharib, 1991; Westerweel, 1997). Measurements were conducted in an indoor pool (1.45 m x 1.0 m, L x W with a depth of 0.6 m) with constantly low background flow. The water was seeded with polyamide particles (Vestosint 1101, Degussa-Hüls AG, Marl, Germany; density: 1.02 g mm^{-2}, median particle size: 74 ± 5 µm) which are naturally buoyant and thus followed the flow of the generated vortex ring. The particles were illuminated by an optically pumped semiconductor laser (Taipan, Coherent, Santa Clara, CA, USA, distributed by Lightline, Osnabrück, Germany; maximum output power 10 W) in constant wave mode, whose beam was passed through a cylindrical lens, thereby spreading the light into a thin horizontal sheet about 1 mm thick and several dm wide. The laser light plane was targeted via mirrors at the middle of the aperture of the blend to allow cross sectional measurements of the vortex rings. A tripod with a high speed camera (Phantom

V12.1, Vision Research Inc., Wayne, NJ USA) was mounted above the pool and recorded the illuminated particles with images of 1280 x 800 pixels at a frequency of 1000 images s^{-1}. The top-view images had a size of 34 cm x 21.5 cm, which resulted in a spatial resolution of 1 pixel representing a space of 0.27 mm x 0.27 mm. In the camera's field of view, the water surface was covered with a Perspex frame (60 x 50 cm, L x W) to prevent image distortions caused by surface waves. Each PIV measurement started with recording the background flow for 5 s. Subsequently, a vortex ring was generated and filmed while it travelled over a distance of 30 cm, plus an additional second to record the wake of the vortex ring. The wake was determined to be negligible due to the comparatively low flow velocities and will not be discussed further. Recorded images were transferred to a hard disc via Ethernet connection and stored uncompressed. For further analysis, the recordings were digitally cut into 25 image pairs per second with a time difference of 1 ms within each pair (free software Virtual Dub 1.8.8. by Avery Lee).

The software DaVis 7.2 (LaVision GmbH, Göttingen, Germany) was used to calculate the flow velocity vectors by conducting a subimage cross-correlation (Willert and Gharib, 1991). According to this method, the most probable average particle displacement is calculated for a group of particles within a particular region of the illuminated flow field between two successive subimages. The subimages used for the cross-correlation, the interrogation areas, had a size of 32 x 32 pixels to 16 x 16 pixels with an overlap between the subimages of 50% for maximum spatial resolution. This resulted in velocity vector fields of 164 x 102 vectors which were then post-processed by validation of the correlation peaks based on the relative correlation height. In addition, the vector fields were smoothed with a moving average filter.

The data from DaVis were then exported in Tecplot format, imported into Matlab 6.5 (MathWorks Inc., Natick, MA, USA) and analysed using custom-made programs to conduct all further calculations of the vortex ring parameters. Every vortex ring was analysed regarding its size, maximum flow velocity, travel velocity, and acceleration. Additionally, reproducibility of the vortex rings was verified.

Vortex ring form

Three profiles of the vortex ring (Fig. 3A: vortex ring S2) were plotted according to Spedding (1987) and Müller et al. (1997), to analyse its form. One vorticity profile was taken along the x'-axis, through the midpoint of one vortex core (Fig. 3B). Two velocity profiles were taken, one along the x'-axis (Fig. 3C) and one along the y'-axis (Fig. 3D), which connects the two counter-rotating vortices of the ring, perpendicular to the x'-axis. The radius of the vortex core (R_0), that is half the distance between the velocity peaks in Fig. 3C, and additionally the ring radius (R), that is half the distance between the outer velocity peaks of the vortex ring minus the core radius (compare Fig. 3D), were measured.

Vortex ring size

For vortex ring size analysis, vectors with a velocity of 0.04 m s^{-1} in the cross section of the vortex ring (see Fig. 3D) were defined as the outer borders of the vortex ring. This velocity was chosen because it was both clearly above background noise and above the detection threshold of the experimental animals. The distance between two opposite vectors meeting the defined velocity criteria was evaluated. The size of the vortex ring was calculated for each vector image by averaging the 10 highest distances along the travel path. This calculated size was again averaged from all vector images along the travel path of the vortex ring within the area of 200 mm up to 315 mm from the aperture, herein after referred to as the mean vortex ring size. The gap of 200 mm before taking data into account is owed to the formation process of the vortex ring. Fish-generated vortex ring size in the literature is generally given as half the distance between vortex ring cores. Our vortex ring diameter is defined as the width of the area above a flow speed of 0.04 m s^{-1} to address the width of the flow structure that impinges on the seal's vibrissae. This area exceeds both cores of the vortex ring.

Maximum flow velocity

The maximum flow velocity within the jet of the vortex ring and its decline along the travel path were calculated by averaging the 10 highest velocity vectors in each recorded vector image within an area of 100 mm up to 315 mm from the aperture. The maximum velocities were calculated at two defined positions along the

travel path for each vortex ring using a linear regression. The first position, 23 cm from the aperture, is defined as the earliest position where the vortex rings impinged on the vibrissae of the animal in the psychophysical experiment. The second position, 34 cm from the aperture, was chosen to cover the complete array where the stimulation of the vibrissae occurred.

Travel velocity

Travel velocity of the vortex ring was measured by comparing its position on the travel path in consecutive images (time space between images was 40 ms ≙ every 40^{th} vector field, 25 vector fields s^{-1}). The y'-axis through the centres of the two counter-rotating vortices was set as the position of the vortex ring (see Fig. 3A). A linear regression for the travel velocities along the travel path was calculated and used to determine the travel velocities at position 23 cm and 34 cm from the aperture.

Acceleration and stimulus duration

The acceleration of the vortex ring was determined by plotting the travel velocity against time and calculating a linear regression. The slope showed the acceleration of the vortex ring. A linear regression was assumed to hold true for the short distance investigated along the travel path. The stimulus duration was set as the time the vortex ring needed to travel from position 23 cm to position 34 cm.

Reproducibility

Exemplarily, one of the 10 stimuli (S9) was recorded five times consecutively on one day with a background noise of 2.137 ± 0.341 mm s^{-1} water velocity (mean ± s.d.). The maximum flow velocities along the vortex ring's travel path and its deviation from the average maximum flow velocity for each position on the travel path were calculated for each recording. The reproducibility was determined through the weighted standard deviation.

Stability of vortex rings

Vortex ring properties (size, maximum flow velocity, travel velocity, and acceleration) were calculated from measurements conducted in an indoor pool to obtain data in constantly low background flow. In the experimental outdoor pool,

background flow was variable due to environmental influences such as wind and movement of the ship (see experimental setup). Trials with uranine-stained vortex rings (see experimental setup) showed that the vortex rings were stable and reached the position of the seal's vibrissae in the behavioural experiment.

Experimental subjects

The test animals were two experimentally naïve male harbour seals (*Phoca vitulina*, L.), named Filou and Moe, both born (in 2006) in captivity. At the time of data acquisition, they were kept with six other harbour seals and a South African fur seal (*Arctocephalus pusillus pusillus*). The animals were fed with freshly thawed fish (1.5 - 3 kg of cut herring or sprats per day), supplemented with vitamins, and received approximately 80% of their daily diet during experimental sessions as primary reinforcement. Typically, experiments were conducted once a day, five days per week. All experiments were conducted in accordance with the German animal protection law.

Experimental setup

The present study was conducted at the “Marine Science Center” (Rostock, Germany). The main animal enclosure was a mesh-surrounded area of 1800 m² with a maximum depth of 6 m. It was located within a marina, thus constantly providing fresh seawater. Floating pontoons offered space for the animals to haul out. A moored ship (length 40 m) served as the office building and laboratory space. On the rear deck of the ship, a separate pool filled with water from the marina served as the experimental pool. This experimental pool could only be reached by the test subjects via a ramp, thereby providing separation from the other animals.

The outdoor testing pool had proportions of 2.3 m x 2.3 m (L x W), with a depth of 1 m (Fig. 1B). It was separated by a wooden board into a compartment for the seal and a test compartment where the vortex rings were generated. A circular opening (30 cm in diameter) in the wooden board allowed the seal to enter the test compartment up to its pectoral flippers. The animal had to position its head through a hoop station and bite on a bite target (food save polyurethane). Both the hoop station and the bite target ensured a consistent head position in every trial and restricted the animal from moving its head during stimulus presentation. In the seal’s compartment,

a start station (yellow plastic sphere) was mounted directly above the water surface, above the opening of the board. Furthermore, two underwater response targets (green plastic spheres) were fixed to the wooden board, one on either side of the opening. Two timber planks (2.95 m x 0.3 m, L x W) served as platforms for the experimenter and the assistant and were positioned across the pool above the test compartment (not shown in the figure). The testing pool was surrounded by a transparent Makrolon wind shield, covering the west and the north side of the pool to screen the water surface from being stirred by the wind.

Two VRGs were fixed on a semi-circular horizontal profile (diameter 1.8 m) made of aluminium. The angular position of the VRGs along the profile could be varied without changing the distance of the aperture of the blend to the bite target (30 cm). The height of the aperture (50 cm above the pool ground) was at the same level as the bite target. The VRGs could be rotated about their vertical axes within the mounting at the angular positions. Two laser pointers, which were fixed underneath the VRGs, beamed at a reflecting band on the wooden board with marks at defined positions. Reproducible conditions in every trial were achieved by orienting the VRGs towards these defined positions via the laser pointers. Occasionally, in some sessions the water within the cubes was stained with uranine (Fluorescein Sodium $C_{20}H_{10}Na_2O_5$, Kremer Pigmente GmbH & Co. KG, Germany) to visualise the vortex rings during the experiment.

Psychophysical procedure

1. Pre-training

Prior to data acquisition, the animals were trained to learn the experimental procedure. Every trial began with blindfolding the seal with a visually opaque elastic mask, which left the mystacial vibrissae uncovered. The blindfolded seal then had to press its snout against the start station, where it was supplied with headphones transmitting pink noise for acoustical masking (Fig. 1C). Upon removal of the headphones, the animal submerged and stationed underwater on the bite target (Fig. 1D). The test animals were trained in two ways to indicate the side on which a hydrodynamic stimulus impinged on its vibrissae, according to a two-alternative forced choice procedure. One animal, Filou, was first actively touched underwater with one of two paddles, either on the right or the left vibrissal pad. Once he had

learned to push his snout on the corresponding response targets (Fig. 1E) upon tactile perception, the paddles were moved close to the vibrissae, but not actually touching the vibrissae anymore, thus creating a hydrodynamic stimulus. The other animal, Moe, started with hydrodynamic stimuli generated with the VRGs, but they were manually operated instead of motor driven, generating strong and irreproducible water disturbances. After the pre-training, the VRGs were operated by motors as described above.

2. Experiment 1: Unilateral stimulation – Detection of single vortex rings

In a first set of experiments, the VRGs were mounted at an angle of 60° on either side of the point directly ahead of the animal's bite target. The task of the blindfolded, stationary harbour seal was to detect the direction (either left or right) from which a single vortex ring impinged on its vibrissae. Every trial started with the visual and acoustical masking of the seal via the mask and headphones. The VRGs were then rotated by an assistant so that one of the two VRGs was oriented towards the bite target, thus producing a vortex ring travelling to the seal's ipsilateral mystacial vibrissal pad (see Fig. 1B and compare travel path 1 in Fig. 2). The other VRG was oriented to generate a vortex ring that travelled to the rear wall of the pool, away from the seal, and did not stimulate the vibrissae. Even if the side of hydrodynamic stimulation did not change in consecutive trials, both VRGs were consistently rotated prior to each trial to create the same noise and water disturbance. After aligning the generators, we imposed a delay of at least 5 s to obtain calm water conditions. As soon as the headphones were removed, the seal submerged and stationed at the bite target (Fig. 1D). Another minimum delay of 10 s was set to reobtain calm water conditions in the test compartment prior to vortex ring generation. Both VRG motors were operated simultaneously by an assistant to avoid giving the animal secondary directional cues due to motor noise. After the vortex ring had impinged on the mystacial vibrissae, a short whistle was given, whereupon the seal was allowed to move its head out of the test compartment to touch the left or the right response target with its snout (Fig. 1E). In case of a correct response, the seal was rewarded with fish.

The experiment was conducted double-blind. The experimenter handling the animal visually checked the orientation of the VRGs behind her back only after the seal had given its response. One session with 30 trials was conducted per day. In

every session, two stimuli were presented pseudorandomly following the principles established by Gellermann (1933), modified according to Holt and Schusterman (2002). The vortex ring impinging on the vibrissae was equally often generated by the right and the left VRG and each vortex ring was presented 15 times per session. A total of ten stimuli (S1 – S10) were presented following this procedure.

2.1. Control experiments – Experiment 1

To exclude the possibility that the animals could have used secondary cues for their decision, two sets of control experiments were carried out after the completion of the data acquisition. Both control experiments were conducted in the exact same manner as the test experiments.

Masked vibrissae

In the first set of control experiments, the possibility that the animals could have successfully completed the task by using a different sense (audition, taste) than the vibrissae was excluded. In addition to the blindfold, the seals had to wear a nylon stocking mask which covered their mystacial vibrissae but was permeable by water and allowed the animal to perceive chemosensory cues. For this control experiment, four different vortex rings (S1, S2, S6, and S9) were presented in three consecutive sessions comprising a total of 30 trials.

Pressure wave

The second set of control experiments was designed to exclude the possibility that the seal's response was based on pressure wave detection instead of vortex ring detection. For this purpose, the apertures of the blends of the VRGs were covered with a thin sheet of latex. This way, a pressure wave was generated, as it was when the apertures were uncovered, but no vortex ring was generated. Seven vortex rings (S1 – S7) were presented this way with 30 trials each.

3. Experiment 2: Bilateral stimulation – Minimum hydrodynamically perceivable angle (MHPA)

In a subsequent set of experiments, the minimum angle from which the direction of a vortex ring is still detectable by the vibrissal system was determined by gradually decreasing the angle between the VRGs. This angle, termed the "minimum

hydrodynamically perceivable angle" (MHPA), was experimentally investigated in accordance with the underwater minimum audible angle of harbour seals (Bodson et al., 2007). The experimental procedure followed that of the previous set of experiments except that the vortex ring would not impinge unilaterally on one of the two vibrissal pads but centrally in the middle of the snout, thus stimulating the vibrissae of both vibrissal pads (bilateral stimulation, compare travel path 2 in Fig. 2). Five of the previously presented vortex rings (S1, S2, S6, S9, and S10) were chosen for this experiment. Each session consisted of 30 trials, and every vortex ring was presented 45 times in total. The data for each stimulus per angular position was pooled from two sessions. One session consisted of 30 trials with constant stimuli (just one stimulus) and one session was a mixed session in which two vortex rings were presented pseudorandomly with 15 trials each.

4. Experiment 3: Contralateral stimulation - Travel direction detection

In a third experiment, the VRGs were fixed at an angle of 17° on either side of the point straight ahead of the animal, but they were rotated within their mounting to create four potential vortex ring travel paths for each VRG (Fig. 2). Travel path 1 led to unilateral and ipsilateral stimulation, as performed in experiment 1, where the vortex ring was generated by the VRG located on the same side as the stimulated mystacial pad. The vortex ring of travel path 2 stimulated the vibrissae bilaterally like in experiment 2. Travel paths 3 and 4 were established to stimulate the vibrissae again unilaterally, however these paths resulted in contralateral mystacial pad stimulation. The vortex ring of travel path 3 was aimed close to the middle of the snout, stimulating also the medial microvibrissae. The lateral macrovibrissae of the contralateral vibrissal pad were stimulated by a vortex ring travelling along path 4. The task of the animal (Filou) was to detect the direction from which a single vortex ring impinged on its vibrissae and thus determine the vortex ring's travel direction. Consequently, it was no longer sufficient to correctly fulfil the task if the seal indicated the side of the mystacial pad where the vortex ring had been perceived. The harbour seal had to analyse the vortex ring regarding its travel direction within the mystacial pad.

Each day one session with 36 trials was conducted including nine trials per travel path with stimulus S9. The first five sessions were conducted in the same manner as the previous two experiments including the blindfold to expose the spontaneous reaction of the harbour seal to the new task. Thereafter, a learning phase followed in which the harbour seal performed the experiment without the blindfold and was able to use vision (the orientation of the VRGs) as a secondary cue for learning purposes. Once the animal had learned the task, it had to perform the task blindfolded again, ensuring that it had learned to respond to the hydrodynamic stimulus and not the visual cue.

4.1. Transfer test

In experiment three, the vortex rings reached the ipsilateral vibrissae earlier than the contralateral vibrissae. Knowing this, the animal could have responded to the vortex rings of the different travel paths by measuring the time between the sound of the generation of the vortex ring and the first impingement on the vibrissae. To show that the response of the animal was not based on the travel duration of the vortex ring, but its travel direction, we presented different stimuli (S1, S2, S9, and S10) with different travel velocities. These four vortex rings were presented equally often and pseudorandomly distributed within five sessions, including 45 trials per travel path and stimulus.

4.2. Control experiments – Experiment 3

Masked vibrissae

Again, the experiment was conducted with masked vibrissae as a control, as described earlier. This time, one session consisted of 18 trials with free vibrissae and 18 interspersed trials with the vibrissae covered by a mask. In total, 10 sessions resulted in 45 trials per travel path in each condition (vibrissae masked and unmasked). The trials of the unmasked condition were used to evaluate, as well as to maintain, the general motivation of the animal to work under masked vibrissae conditions.

New travel path –1

A new travel path (path –1 in Fig. 2) was introduced so that the right VRG stimulated the vibrissae of the right vibrissal pad with a vortex ring travelling contralaterally, from left to right, through the mystacial pad (corresponding procedure for the left VRG and left vibrissal pad, respectively). In this case, the animal had to respond by touching the left response target because the travel direction was from left to right. This control path was included in order to exclude a potential secondary cue that might have originated from the VRG that was aimed towards the animal and had generated the stimulus travelling towards the vibrissae. The VRG was fixed straight ahead of the animal and could not deliver a positional cue. Only vortex ring S9 was presented in five sessions with 36 trials per day resulting in 45 trials for travel paths –1, 2, and 4. Travel paths 1 and 3 were unequally presented, 15 and 30 times, respectively.

New travel path 1*

Once more a new travel path (path 1* in Fig. 2) was included in the session to rule out that the animal had learned to respond on the contralateral response target if it perceived a vortex ring stimulating the lateral macrovibrissae. For this purpose, the vortex ring of travel path 1* stimulated the lateral macrovibrissae similar to the vortex ring of travel path 4. However, instead of a contralateral impingement, it was perceived ipsilaterally. The trials of travel path 1* superseded those of travel path 1 resulting in 45 trials for each of the 4 travel paths (1*, 2, 3, and 4) over five sessions. Again, only S9 was presented in this condition.

RESULTS

Vortex ring characterisation

PIV measurements showed that the stimuli generated by the VRGs were vortex rings, as they consisted, in cross section, of two counter-rotating vortices with a median laminar jet flow directed in the travel direction (see Fig. 3A). Within this central laminar jet flow the highest velocities were found. The velocity and vorticity profiles of the generated vortex ring (see Fig. 3B-D) showed that the cross sections

of the vortex ring were similar to a Rankin vortex ring, as it has been described for fish-generated vortex rings (compare Spedding, 1987 and Müller et al., 1997). Like Rankin vortex rings, the cross sections consisted of a vortex core, which was in solid-body rotation, while the surrounding region was almost free of vorticity. Maximum vorticity within the core of S2 was 33.96 s^{-1} (see Fig. 3B). Velocity (see Fig. 3C) was zero in the centre of the vortex core and increased linearly to the outer edge. The velocity peaks display the outer edges of the vortex core. The curvilinear decrease in velocity marks the surrounding potential flow region. The radius of the core (R_0) was 5.21 mm and the ring radius (R) was 11.97 mm. The measurements regarding the reproducibility of the stimuli using five repetitions of the same stimulus revealed that maximum flow velocities in the vortex ring jets, averaged over the positions along the path, had a weighted standard deviation of 0.136 m s^{-1}. Travel velocities of the vortex rings averaged over the positions along the path for the five measurements had a weighted standard deviation of 0.061 m s^{-1}. The properties of the 10 vortex rings used in the behavioural experiments are shown in Tab. 1.

Psychophysical experiments

1. Pre-training

Both animals learned to indicate the side on which they had perceived a hydrodynamic stimulus, either generated by a paddle or manually by a VRG, within 100 trials. Both animals showed fast and discontinuous learning. Moe increased his performance from constantly 50% correct choices (chance level) due to 100% side preference to the left, in the first five sessions with 20 trials each, to 85% correct choices (χ^2-test, $P>0.01$, $N=20$) in the sixth session. The learning curve for Filou was similar but with variable session lengths.

2. Experiment 1: Unilateral stimulation – Detection of single vortex rings

Fig. 4 shows the performance of both animals in the ipsilateral stimulation task as a function of the 10 presented stimuli. The overall performance for indicating the side of perception of the vortex ring was highly significant for all vortex rings (above 97.78% correct choices, χ^2-test, $P<0.001$, $N=45$). The experiment was conducted until the performance reached its maximum with no further improvement from one session to the next. Fig. 4 shows the pooled data of the last three sessions and thus

the maximum consistent performance acquired as a basis for the subsequent analysis of the MHPA. In general, no significant difference (two tailed *t*-test with equal variances: P>0.05) in the performance of the detection of vortex rings differing in size and velocity was found when comparing both animals.

2.1. Control experiments – Experiment 1

Masked vibrissae

The control experiments, conducted directly after data acquisition, revealed that the animals solved the task by using hydrodynamic perception by the mystacial vibrissae. The performance of both seals dropped immediately to chance level when a nylon stocking mask covered the vibrissae (Moe 50% and Filou 36.67% correct choices; χ^2-test, $P>0.05$, $N=30$). In two of the first three trials, Filou left the bite target and came up to the water surface without responding at one of the two response targets. Filou had not shown this behaviour in any of the trials before, which suggests he was confused about the "missing" stimulus. These two trials were counted as incorrect.

Pressure wave

The second type of control trials confirmed that the response was based on vortex ring perception as the performance dropped to chance level in those trials where only a pressure wave developed (vortex ring inhibited by a latex sheet, see materials and methods). Overall performance for all seven vortex rings (S1 – S7) was 55.33% correct choices for Moe (χ^2-test, $P>0.05$, $N=150$) and 56.67% correct choices for Filou (χ^2-test, $P>0.05$, $N=150$) in five sessions. Contrary to normal trials, in 28% and 20% of the control trials more than one whistle (up to four whistles) was necessary to trigger Moe and Filou, respectively, to leave the bite target and give a response.

3. Experiment 2: Bilateral stimulation – Minimum hydrodynamically perceivable angle (MHPA)

Fig. 5 illustrates the animals' performance plotted against the angular position of the VRGs for all six stimuli. Each bar shows pooled data of two sessions, resulting in 45 trials. Moe's performance remained at a highly significant level in every session

for all vortex rings when decreasing the angle of the VRGS on either side of the animal from 60° to 5.7° (χ^2-test, P<0.001, N=30). Filou's performance was highly significant (86.67% correct choices or higher; χ^2-test, P<0.001, N=30) in each session until the angle was reduced from 17° to 9.5°. It took 80 trials (three sessions, of which the second one was shortened from 30 to 20 trials due to lack of cooperation from the animal) with performance at chance level until Filou's performance was back at a highly significant level (93.33% correct choices; χ^2-test, P<0.001, N=30). These three sessions are excluded from the data shown in Fig. 5 because they would distort the animal's actual perception capacity.

Fig. 6 shows the performance of both seals averaged over all stimulus types plotted against the angular positions of the VRGs. For both seals, performance decreased from nearly 100% correct choices at 60° angular position to 91.11% (Filou: $r_S(4)=0.943$, P=0.01) and 89.44% (Moe: $r_S(4)=0.943$, P=0.01) at 5.7°, but still remained highly significant (χ^2-test, P<0.001, N=180 (Moe: four different stimuli) and N=225 (Filou: five different stimuli), respectively). The decrease in performance did not correlate with the performance regarding each vortex ring (two tailed t-test with equal variances: P>0.01).

4. Experiment 3: Contralateral stimulation - Travel direction detection

The animal's ability to analyse the travel direction of the perceived vortex ring is shown in Fig. 7. Each session block consists of pooled data of five consecutive sessions, showing the performance for each of the four travel paths (45 trials per data point). The spontaneous reaction of Filou to the new test situation, where he was blindfolded in the first five sessions, resulted in performance at chance level when taking all four travel paths into account. Filou responded 100% correctly when the vortex ring was perceived ipsilaterally (path 1), and he responded correctly in all but four trials when his vibrissae were stimulated bilaterally (path 2). The contralateral stimulation of travel path 4 led to 100% incorrect responses, showing that Filou responded to the corresponding side where the vortex ring had been perceived. Filou showed the same response behaviour for vortex rings of travel path 3 except for nine trials in which he gave a correct response. After five sessions, the experiment was continued without the blindfold to facilitate learning. It took Filou 35 sessions (seven session blocks) to reach the learning criterion of at least 80% correct

choices for all four travel paths in three consecutive sessions. Ten sessions of overtraining followed in which Filou did not yet wear a blindfold. The performance stayed at a highly significant level (χ^2-test, P<0.001, N=45) for travel paths 1 to 3. Performance for travel path 4 dropped to 71.11% correct choices (still statistically significant: χ^2-test, P<0.01, N=45) in session block 9 before increasing again to highly significant performance at 77.78% correct choices (χ^2-test, P<0.001, N=45). The first five sessions during which Filou was blindfolded (session block 11) showed a drop in performance again for travel path 4 (68.89% correct choices: χ^2-test, P<0.05, N=45) and highly significant performance for travel paths 1, 2, and 3. The following data points of each travel path of session block 12 consist only of four sessions that were conducted during moulting when the lateral macrovibrissae of both mystacial pads were already shed and/or still shedding. With increasing number of missing vibrissae, Filou's performances in each session for travel paths 3 and 4 decreased drastically. Thus, the animal's performance within the four pooled sessions was at chance level with 71.43% (χ^2-test, P>0.05, N=21) and 36.84% (χ^2-test, P>0.05, N=19) correct choices, respectively. Performance for travel path 1 decreased slightly but remained highly significant (85.71%; χ^2-test, P<0.001, N=21). The loss of the lateral macrovibrissae did not affect the performance for travel path 2 (100%; χ^2-test, P<0.001, N=20) where the vortex ring was aimed at the medial microvibrissae. The experiment was suspended until the moulting was complete and the vibrissae had grown back to their normal length. Consequently, upon resuming the experiment (session block 13), the performances for all four travel paths were back at a highly significant level.

4.1. Transfer test

When vortex rings with different velocities were introduced, the performance of the seals (S1, S2, S9, and S10) for all four travel paths remained at a highly significant level (χ^2-test, P<0.001, N=45; session block 14). A slight decrease in overall performance for each travel path was found (two tailed t-test with equal variances: P=0.036), but did not correlate with the performance regarding each vortex ring (two tailed t-test with equal variances: P>0.05).

4.2. Control experiments – Experiment 3

Masked vibrissae

The control experiment with mixed trials of unmasked and masked vibrissae (data not shown in Fig. 7) showed that the vibrissal system is indispensable in order to solve the task. While the performance in the unmasked trials remained highly significant (path 1: 82.22%, path 2: 97.78%, path 3: 100%, path 4: 95.56%; χ^2-test, $P<0.001$, $N=45$), in the masked condition, Filou was not able to distinguish the correct travel direction of the vortex rings (path 1: 42.22%, path 2: 55.56%, path 3: 46.67%, path 4: 48.89%; χ^2-test, $P>0.05$, $N=45$).

New travel path –1

The performance for the new travel path -1 is shown in Fig. 7, session block 15, as a triangle. With an overall performance of 91.11% correct choices, this result is highly significant (χ^2-test, $P<0.001$, $N=45$) similar to the performances for all other travel paths tested in this session block (travel path 1: 100% ($N=15$), path 2: 95.56% ($N=45$), path 3: 100% ($N=30$), path 4: 97.78% ($N=45$); χ^2-test, $P<0.001$). Already in the first session of this session block, Filou responded correctly in eight out of nine trials of this novel travel path (88.89%; χ^2-test, $P<0.05$).

New travel path 1*

Again, when introduced to a novel travel path (travel path 1*, see Fig. 7: diamond; session block 16), Filou distinguished the travel direction of the perceived vortex ring with a highly significant performance of 95.56% correct choices (χ^2-test, $P<0.001$, $N=45$). Filou responded 100% correctly in the first session of this session block (χ^2-test, $P<0.01$, $N=9$). For both travel path 2 and travel path 3, Filou responded incorrectly only once out of 45 trials (97.78%; χ^2-test, $P<0.001$). Regarding the performance for travel path 4, Filou showed the best performance in this last session block altogether (100%; χ^2-test, $P<0.001$, $N=45$).

DISCUSSION

Comparison with fish-generated vortex rings

In general, the stimuli used in this study resemble those found in fish wakes with regard to form, size, and velocity. First, the form of the vortex rings in this study resembled Rankine vortex rings, which are defined by a profile of constant vorticity in the cores and no vorticity in the periphery; the same vortex ring type that has been described in fish wakes (Blickhan et al., 1992; Müller et al., 1997; Hanke et al., 2000).

Second, the sizes of the vortex rings utilised in our experiments correspond well with the wide range of sizes of fish-generated vortex rings that occur in nature. Due to the difference in vortex ring size definition when comparing fish-generated vortex rings from literature with our artificially generated vortex rings, the mentioned sizes of fish-generated vortex rings are underestimated compared to size measurements performed with our measuring procedure. For example, vortex ring S2 has a core to core radius of 11.97 mm (23.94 mm in core to core diameter) but a vortex ring diameter according to our definition (see vortex ring size in material and methods) of 68.95 ± 1.58 mm, which is almost three times larger. Vortex rings shed by a black surfperch (*Embiotoca jacksoni*) of 20 cm total body length (TBL) that swam at 1.5 BL s^{-1} had a core to core radius of 32.1 ± 0.35 mm (mean ± s.e.m.) (Drucker and Lauder, 2000) and are therefore supposed to be larger than our largest vortex ring, S1, which had an overall diameter per our definition of 89.89 ± 3.31 mm (mean ± s.d.) (expecting the overall diameter to be larger than the core to core diameter). At the same swim speed of 1.5 BL s^{-1}, a 20 cm long (TBL) bluegill sunfish generated vortex rings with a 15.4 ± 0.08 mm (mean ± s.e.m.) core to core radius which is again bigger than the smallest vortex ring applied in our experiments (S4: 31.29 ± 1.71 mm in diameter; mean ± s.d.).

Concerning our third property, maximum velocities within the jet of the vortex rings, PIV measurements of the stimuli revealed mean maximum velocities of 2.108 m s^{-1} (S1) down to 0.224 m s^{-1} (S4) in the area of vortex ring impingement on the vibrissae, 23 cm from the aperture of the blend. Maximum flow velocities measured within the generated vortex ring of an escaping rainbow trout (25.5 cm TBL) can

reach up to 1.6 m s^{-1} (Niesterok and Hanke, 2013). A bluegill sunfish, about half as long (11 cm TBL) as the rainbow trout, generates a wake with peak flow velocities of nearly 1 m s^{-1} during a C-start escape response (Tytell and Lauder, 2008). Vortex rings in the present study with high maximum velocities (S1, S2, S3, S5, and S6) represent flow structures naturally found in the wakes of fish performing an escape manoeuvre. Likewise, our vortex ring with the slowest mean maximum velocities (S4: 0.224 m s^{-1}) matched well with the water particle velocities of about 0.23 m s^{-1} generated in a steady swimming (at 25.2 cm s^{-1}) chub mackerel (*Scomber japonicus*) 24 cm in fork length (Nauen and Lauder, 2001).

Ecological relevance of stimuli

Harbour seals are food generalists that forage on seasonally and spatially dominant species (Pierce et al., 1991; Tollit et al., 1997; Sharples et al., 2009). Analyses of harbour seal scats in the Bay of Somme (English Channel, France) revealed that their diet contains pelagic fish such as sardines with a mean size of 18.9 ± 1.6 cm (range 17.0 – 20.7 cm). In one sample, even a mullet of 46.4 cm was found (Spitz et al., 2015). At Dundrum Bay (Minerstone), north-east Ireland, Wilson et al. (2002) showed that harbour seals in that area mostly fed on gadids, including whiting ranging between 10 and 20 cm and haddock, pollack, and saithe ranging mainly between 20 and 40 cm.

The fact that the properties of our artificially generated vortex rings correspond well to those found in natural fish wakes, as well as the finding that the size of fish used in the mentioned fish wake studies matches to those that have been found to be primary food resources for wild harbour seals, show that our research has direct ecological relevance to predator-prey interactions.

Vortex ring detection

Both harbour seals, Filou and Moe, showed highly significant performances in the vortex ring detection task for all vortex rings presented. This high level of performance and the fast learning process of the general task in both animals emphasise that vortex rings, as hydrodynamic stimuli occurring in their natural habitat, provide easily accessible information for harbour seals. The maximum jet

velocities of all vortex rings calculated for the moment of impingement on the vibrissae were above the sensory threshold of the vibrissal system determined for the detection of dipole stimuli (Dehnhardt et al., 1998b). However, dipole stimuli in the experimental design of Dehnhardt et al. had durations of three seconds (rise and fall times 300 ms). In our experiment, the vortex rings were a single hydrodynamic event stimulating the vibrissae in each trial for less than one second (see Tab. 1 for actual duration of stimulation from first impingement until leaving of the vibrissal area). This should lead to different detection thresholds.

The minimum hydrodynamically perceivable angle (MHPA)

Due to technical constraints, a MHPA could not be determined because the performance of both individuals was still highly significant at the smallest adjustable angle of 5.7°. A possible habituation to the stimuli and the decreasing angle cannot be excluded completely but the high level of performance in the task even at this small angle cannot be explained exclusively by habituation. The minimum audible angle (MAA) determined for two harbour seals, measured underwater in the horizontal plane, revealed frequency dependent values with small angles (3.2° and 3.1°) at low frequencies (0.2 kHz) and larger angles (13.5° and 17.4°) at high frequencies (16 kHz) (Bodson et al., 2007). The MHPA does not show this kind of stimulus dependent performance difference (two-tailed *t*-test with equal variances: $P>0.01$). A slight decline in performance with decreasing angles for both animals was found ($r_S(4) = 0.943$, $P=0.01$), however this was not stimulus dependent. Compared to the underwater sound localization acuity at high frequencies, the acuity in hydrodynamically detecting the direction of a vortex ring is much higher. Since the upper limit of the MHPA was not yet reached at an angle of 5.7°, the high performance shown in these data strongly indicate that it might be as low as, or even lower, than the MAA for low frequencies.

Possible mechanisms for the discrimination of the angle of impact for the MHPA

While determining the MHPA, we directed the vortex rings towards the middle of the snout, thus stimulating the vibrissae of both vibrissal pads with a temporal difference and a velocity difference, in principle comparable to the interaural time and

intensity difference in auditory localisation (Mills, 1985). Both the maximum velocity in the central jet of the vortex ring and the travel velocity of the vortex ring decrease with travel distance. These velocity differences and/or the temporal difference could have been used by the harbour seal to analyse the travel direction of the stimuli. This ability would be facilitated by an individual representation of single vibrissa in the brain. For rodents, it is well established that each vibrissal follicle is represented one-to-one in discrete anatomic structures in the brain, “barrelettes” in the brain stem nuclei, “barreloids” in the thalamus, and “barrels” in the somatosensory cortex (Woolsey and Van der Loos, 1970; Weller and Johnson, 1975; Jeanmonod et al., 1977). Recently, barrelette-like structures have been shown in the brain stem of one pinniped species, the California sea lion (Sawyer et al., 2016). The authors argue that it was due to the cutting method of the tissue and the limitation to only one brain that neither a perfect one-to-one correspondence for the barrelette-like structures nor clear vibrissae-related barreloid-like structures in the thalamus could be shown. However, the authors hypothesise that a one-to-one representation of each vibrissa exists in the brainstem, thalamus, and cortex of a California sea lion brain. If a one-to-one mapping from the sensory periphery to the central nervous system is realised in harbour seals, a comparison of hydrodynamic information from one vibrissa to the next in our experiment is likely. Further anatomical research is vital to fully understand the complex representation of the pinniped mystacial vibrissal array in the brain structures.

Travel direction detection

At first, Filou was not able to spontaneously respond correctly to the new experimental task. A possible explanation for this is that Filou had learned in the previous two experiments to respond to the side where the vibrissae were stimulated (experiment 1) or stimulated first (experiment 2). After a comparatively long learning phase, Filou finally showed that he was able to analyse the travel direction of a single vortex ring impinging on his vibrissae, irrespective of the stimulation type, ipsilateral (like in experiment 1), bilateral (like in experiment 2), or contralateral (new stimulation type). Therefore, harbour seals should not only be able to detect the swimming direction and follow the wake of a fish from a complex hydrodynamic trail (Wieskotten et al. 2010b) but also when confronted with only a single vortex ring.

The transfer test showed that Filou's ability to identify the vortex ring's travel direction was independent of the vortex ring parameters as he managed to solve the task with different vortex rings. Control experiment 1 (masked vibrissae) ensured that Filou's vibrissae were imperative to successfully solve the task. Control experiments 2 and 3 (new travel paths) showed that Filou indeed analysed the travel direction of the vortex ring and no potential secondary cues were used.

Conclusion

Harbour seals can detect the moving direction of a complex hydrodynamic trail (Wieskotten et al., 2010b) as well as distinguish between trail generators differing in size and shape (Wieskotten et al., 2011). Until the present study, it could not be clarified which component of this complex hydrodynamic event is used by harbour seals to extract relevant directional information or generator specific information. Wieskotten et al. (2010b) speculated that vortex rings are crucial distinguishing features of the hydrodynamic trail for harbour seals for two main reasons. First, the moving direction of the high velocities of the central jet within the vortex rings offers directional information. Second, in the experiment, the harbour seal's vibrissae always reached areas where vortices and central jets occurred. However, they argue that the harbour seal's vibrissal perception of the hydrodynamic trail is a dynamic process, and other parameters, such as the structure and spatial arrangement of the vortices within the hydrodynamic trail, cannot be excluded as potential influencing factors on the animal's decision in this experiment. In the present experiment, the only available hydrodynamic parameter was a single vortex ring and we showed that this hydrodynamic feature is both perceptible and sufficient for a harbour seal to gain information about the origin of its generator. Harbour seals are able to accurately follow complex hydrodynamic trails similar to those generated by swimming fish (Dehnhardt et al., 2001; Wieskotten et al., 2010b). Our data strongly indicate that if a harbour seal is confronted with only a single vortex ring as a hydrodynamic cue when hunting, it should still be able to distinguish the swimming direction of the fish and thus track it successfully.

ACKNOWLEDGEMENTS

The authors thank the entire team of the Marine Science Center for all the support and P. Kumm for the construction of the custom-made parts of the setup.

COMPETING INTEREST

The authors declare no competing or financial interests.

FUNDING

This work was supported by grants of the VolkswagenStiftung to G.D. and the German Research Foundation (DFG, SPP1207) [HA441/8-1 to W.H. and DE538/9-3 to G.D.].

LIST OF SYMBOLS AND ABBREVIATIONS

MHPA	minimum hydrodynamically perceivable angle
PIV	particle image velocimetry
MAA	minimum audible angle
VRG	vortex ring generator
R_o	ring core radius
R	ring radius
χ^2-test	Chi-squared test
P	p-value
N	number of trials
TBL	total body length
s.e.m.	standard error of the mean
s.d.	standard deviation

REFERENCES

Adrian, R. J. (1991). Particle imaging techniques for experimental fluid mechanics. *Ann. Rev. Fluid Mech*. **23**, 261-304.

Aleyev, Y. G. (1977). *Nekton*. The Hague: Dr W. Junk. 435pp.

Andres, K. H. (1966). Über die Feinstruktur der Rezeptoren an Sinushaaren. *Zeitschrift für Zellforschung* **75**, 339-365.

Bleckmann, H., Breithaupt, T., Blickhan, R. and Tautz, J. (1991). The time course and frequency content of hydrodynamic events caused by moving fish, frogs, and crustaceans. *J. Comp. Physiol. A* **168**, 749-757.

Blickhan, R., Krick, C. M., Zehren, D. and Nachtigall, W. (1992). Generation of a vortex chain in the wake of a subundulatory swimmer. *Naturwissenschaften* **79**, 220-221.

Bodson, A., Miersch, L. and Dehnhardt, G. (2007). Underwater localization of pure tones by harbor seals (*Phoca vitulina*). *J. Acoust. Soc. Am.* **122**, 2263-2269.

Dehnhardt, G. and Dücker, G. (1996). Tactual discrimination of size and shape by a California sea lion (*Zalophus californianus*). *Anim. Learn. Behav*. **24**, 366-374.

Dehnhardt, G. and Kaminski, A. (1995). Sensitivity of the mystacial vibrissae of harbour seals (*Phoca vitulina*) for size differences of actively touched objects. *J. Exp. Biol.* **198**, 2317-2323.

Dehnhardt, G. and Mauck, B. (2008). Mechanoreception in secondarily aquatic vertebrates. In *Sensory evolution on the threshold: adaptations in secondarily aquatic vertebrates* (ed. J. G. M. Thewissen and S. Nummela), pp. 295-314. Berkeley, Los Angeles: University of California Press.

Dehnhardt, G., Hyvärinen, H., Palviainen, A. and Klauer, G. (1999). Structure and innervation of the vibrissal follicle-sinus complex in the Australian water rat, *Hydromys chrysogaster*. *J. Comp. Neurol.* **411**, 550-562.

Dehnhardt, G., Mauck, B. and Bleckmann, H. (1998b). Seal whiskers detect water movements. *Nature* **394**, 235-236.

Dehnhardt, G., Mauck, B., Hanke, W. and Bleckmann, H. (2001). Hydrodynamic trail following in harbor seals (*Phoca vitulina*). *Science* **293**, 102-104.

Dehnhardt, G., Mauck, B. and Hyvärinen, H. (1998a). Ambient temperature does not affect the tactile sensitivity of mystacial vibrissae of harbour seals. *J. Exp. Biol.* **201**, 3023-3029.

Dehnhardt, G., Mauck, B. and Hyvärinen, H. (2003). The functional significance of the vibrissal system of marine mammals. In *The Merkel cell: Structure - development - function - and cancerogenesis* (ed. K. I. Baumann, I. Moll and Z. Halata), pp. 127-135. Berlin, Heidelberg, New York: Springer-Verlag.

Drucker, E. G. and Lauder, G. V. (2000). A hydrodynamic analysis of fish swimming speed: Wake structure and locomotor force in slow and fast labriform swimmers. *J. Exp. Biol.* **203**, 2379-2393.

Dykes, R. W. (1975). Afferent fibers from mystacial vibrissae of cats and seals. *J. Neurophysiol.* **38**, 650-662.

Erdsack, N., Dehnhardt, G. and Hanke, W. (2014). Thermoregulation of the vibrissal system in harbor seals (*Phoca vitulina*) and Cape fur seals (*Arctocephalus pusillus pusillus*). *J. Exp. Mar. Biol. Ecol*. **452**, 111-118.

Gellermann, L. W. (1933). Chance orders of alternating stimuli in visual discrimination experiments. *J. Genet. Psychol*. **42**, 206-208.

Ginter, C. C., DeWitt, T. J., Fish, F. E. and Marshall, C. D. (2012). Fused traditional and geometric morphometrics demonstrate pinniped whisker diversity. *PLoS ONE* **7** (4), 1-10.

Ginter Summarell, C. C., Ingole, S., Fish, F. E. and Marshall, C. D. (2015). Comparative analysis of the flexural stiffness of pinniped vibrissae. *PLoS ONE* **10** (7), 1-15

Gläser, N., Wieskotten, S., Otter, C., Dehnhardt, G. and Hanke, W. (2011). Hydrodynamic trail following in a California sea lion (*Zalophus californianus*). *J. Comp. Physiol. A* **197** (2), 141-151.

Grant, R., Wieskotten, S., Wengst, N., Prescott, T. and Dehnhardt, G. (2013). Vibrissal touch sensing in the harbor seal (*Phoca vitulina*): How do seals judge size? *J. Comp. Physiol. A* **199** (6), 521-533.

Hanke, W. and Bleckmann, H. (2004). The hydrodynamic trails of *Lepomis gibbosus* (Centrarchidae), *Colomesus psittacus* (Tetraodontidae) and *Thysochromis ansorgii* (Cichlidae) measured with Scanning Particle Image Velocimetry. *J. Exp. Biol.* **207**, 1585-1596.

Hanke, W., Brücker, C. and Bleckmann, H. (2000). The ageing of the low-frequency water disturbances caused by swimming goldfish and its possible relevance to prey detection. *J. Exp. Biol.* **203**, 1193-1200.

Hanke, W., Witte, M., Miersch, L., Brede, M., Oeffner, J., Michael, M., Hanke, F., Leder, A. and Dehnhardt, G. (2010). Harbor seal vibrissa morphology suppresses vortex-induced vibrations. *J. Exp. Biol.* **213**, 2665-2672.

Hill, M. J. M. (1894). On a spherical vortex. *Phil. Trans. R. Soc. A* **185**, 213-245.

Holt, M. M. and Schusterman, R. J. (2002). Seals, sequences, and signal detection. *Mar. Mamm. Sci.* **18**, 994-998.

Hyvärinen, H. and Katajisto, H. (1984). Functional structure of the vibrissae of the ringed seal (*Phoca hispida* Schr.). *Acta Zool. Fenn.* **171**, 27-30.

Hyvärinen, H., Palviainen, A., Strandberg, U. and Holopainen, I. J. (2009). Aquatic environment and differentiation of vibrissae: Comparison of sinus hair systems of ringed seal, otter and pole cat. *Brain Beh. Evol.* **74**, 268-279.

Jeanmonod, D., Rice, F. L. and Van Der Loos, H. (1977) Mouse somatosensory cortex: Development of the alterations in the barrel field which are caused by injury to the vibrissal follicles. *Neurosci. Lett.* **6**, 151–156.

Kastelein, R. A. and van Gaalen, M. A. (1988). The sensitivity of the vibrissae of a Pacific walrus (*Odobenus rosmarus divergens*) Part 1. *Aquat. Mamm.* **14**, 123-133.

Lauder, G. V. and Drucker, E. G. (2002). Forces, fishes, and fluids: Hydrodynamic mechanisms of aquatic locomotion. *News Physiol. Sci.* **17**, 235-240.

Ling, J. K. (1966). The skin and hair of the southern elephant seal, *Mirounga leonina* (Linn.). *Aust. J. Zool.* **14**, 855-866.

Ling, J. K. (1972). Vibrissa follicles of the Ross seal. *Antarct. Sci.* **27**, 19-24

Ling, J. K. (1977). Vibrissae of marine mammals. In *Functional Anatomy of Marine Mammals*, (ed. R. J. Harrison), pp. 387-415. London: Academic Press.

Marshall, C. D., Amin, H., Kovacs, K. M. and Lydersen, C. (2006). Microstructure and innervation of the mystacial vibrissal follicle-sinus complex in bearded seals, *Erignathus barbatus* (Pinnipedia: Phocidae). *Anat. Rec. Part A* **288A**, 13-25.

Marshall, C. D., Rozas, K., Kot, B. and Gill, V. (2014). Innervation patterns of sea otter (*Enhydra lutris*) mystacial follicle-sinus complexes. *Front. Neuroanat*. **8**, 121.

Mattson, E. E. and Marshall, C. D. (2016). Follicle microstructure and innervation vary between pinniped micro- and macrovibrissae. *Brain Beh. Evol.* **88**, 43-58.

McGovern, K. A., Marshall, C. D. and Davis, R. W. (2014). Are vibrissae viable sensory structures for prey capture in Northern elephant seals, *Mirounga angustirostris*? *Anat. Rec.* **298**, 750-760.

Miersch, L., Hanke, W., Wieskotten, S., Hanke, F. D., Oeffner, J., Leder, A., Brede, M., Witte, M. and Dehnhardt, G. (2011). Flow sensing by pinniped whiskers. *Phil. Trans. R. Soc. B* **366**, 3077-3084.

Mills, A. W. (1985). On the minimum audible angle. *J. Acoust. Soc. Am.* **30**, 237-246.

Müller, U. K., Smit, J., Stamhuis, E. J. and Videler, J. J. (2001). How the body contributes to the wake in undulatory fish swimming: Flow fields of a swimming eel (*Anguilla anguilla*). *J. Exp. Biol.* **204**, 2751-2762.

Müller, U. K., Stamhuis, E. J. and Videler, J. J. (2000). Hydrodynamics of unsteady fish swimming and the effects of body size: Comparing the flow fields of fish larvae and adults. *J. Exp. Biol.* **203**, 193-206.

Müller, U. K., van den Heuvel, B. L. E., Stamhuis, E. J. and Videler, J. J. (1997). Fish foot prints: Morphology and energetics of the wake behind a continuously swimming mullet (*Chelon labrosus risso*). *J. Exp. Biol.* **200**, 2893-2906.

Nauen, J. C. and Lauder, G. V. (2001). Locomotion in scombrid fishes: Visualization of flow around the caudal peduncle and finlets of the chub mackerel *Scomber japonicus*. *J. Exp. Biol.* **204**, 2251-2263.

Nauen, J. C. and Lauder, G. V. (2002). Hydrodynamics of caudal fin locomotion by chub mackerel, *Scomber japonicus* (Scombridae). *J. Exp. Biol.* **205**, 1709-1724.

Niesterok, B. and Hanke, W. (2013). Hydrodynamic patterns from fast-starts in teleost fish and their possible relevance to predator–prey interactions. *J. Comp. Physiol. A* **199**, 139-149.

Pierce, G. J., Thompson, P. M., Miller, A., Diack, J. S. W., Miller, D. and Boyle, P. R. (1991) Seasonal variation in the diet of common seals (*Phoca vitulina*) in the Moray Firth area of Scotland, *J. Zool.* **223**, 641-652.

Rayner, J. M. V. (1995) Dynamics of the vortex wakes of flying and swimming vertebrates. In *Biological Fluid Dynamics* (ed. C. P. Ellington and T. J. Pedley), pp. 131-155. Cambridge: Company of Biologist Ltd.

Rice, F. L., Mance, A. and Munger, B. L. (1986). A comparative light microscopic analysis of the innervation of the mystacial pad. I. Vibrissal follicles. *J. Comp. Neurol.* **252**, 154-174.

Rosen, M. W. (1959) *Water flow about a swimming fish*. China Lake, CA: U.S. Naval Ordnance Test Station TP 2298. 96pp.

Sawyer, E. K., Turner, E. C. and Kaas, J. H. (2016). Somatosensory brainstem, thalamus, and cortex of the California sea lion (*Zalophus californianus*). *J. Comp. Neurol.* **524**, 1957-75.

Schulte-Pelkum, N., Wieskotten, S., Hanke, W., Dehnhardt, G. and Mauck, B. (2007). Tracking of biogenic hydrodynamic trails in harbor seals (*Phoca vitulina*). *J. Exp. Biol.* **210**, 781-787.

Sharples, R. J., Arrizabalaga, B. and Hammond, P. S. (2009). Seals, sandeels and salmon: Diet of harbour seals in St. Andrews Bay and the Tay Estuary, southeast Scotland. *Mar. Ecol. Prog. Ser.* **390**, 265-276.

Spedding, G. R. (1987). The wake of a kestrel (*Falco tinnunculus*) in flapping flight. *J. Exp. Biol.* **127**, 59-78.

Spitz, J., Dupuis, L., Becquet, V., Dubief, B. and Trites, A. W. (2015). Diet of the harbour seal *Phoca vitulina*: Implication for the flatfish nursery in the Bay of Somme (English Channel, France). *Aquat. Living Resour.* **28**, 11-19.

Standen, E. M. and Lauder, G. V. (2007). Hydrodynamic function of dorsal and anal fins in brook trout (*Salvelinus fontinalis*). *J. Exp. Biol.* **210**, 325-339.

Stephens, R. J., Beebe, I. J. and Poulter, T. C. (1973). Innervation of the vibrissae of the California sea lion, *Zalophus californianus*. *Anat. Rec.* **176**, 421-441.

Tollit, D. J., Thompson, P. M. and Greenstreet, S. P. R. (1997). Prey selection by harbour seals, *Phoca vitulina*, in relation to variations in prey abundance. *Can. J. Zool.* **75**, 1508-1518.

Tytell, E. D. and Lauder, G. V. (2008). Hydrodynamics of the escape response in bluegill sunfish, *Lepomis macrochirus*. *J. Exp. Biol.* **211**, 3359-3369.

Videler, J. J., Müller, U. K. and Stamhuis, E. J. (1999). Aquatic vertebrate locomotion: Wakes from body waves. *J. Exp. Biol.* **202**, 3423-3430.

Weller, L. W. and Johnson, J. I. (1975) Barrels in cerebral cortex altered by receptor disruption in newborn but not in five-day-old mice (Cricetidea and Muridae). *Brain Res.* **83**, 504–508.

Westerweel, J. (1997). Fundamentals of digital particle image velocimetry. *Meas. Sci. Technol.* **8**, 1379-1392.

Wieskotten, S., Dehnhardt, G., Mauck, B., Miersch, L. and Hanke, W. (2010a). The impact of glide phases on the trackability of hydrodynamic trails in harbor seals (*Phoca vitulina*). *J. Exp. Biol.* **213**, 3734-3740.

Wieskotten, S., Dehnhardt, G., Mauck, B., Miersch, L. and Hanke, W. (2010b). Hydrodynamic determination of the moving direction of an artificial fin by a harbour seal (*Phoca vitulina*). *J. Exp. Biol.* **213**, 2194-2200.

Wieskotten, S., Mauck, B., Miersch, L., Dehnhardt, G. and Hanke, W. (2011). Hydrodynamic discrimination of wakes caused by objects of different size or shape in a harbour seal (*Phoca vitulina*). *J. Exp. Biol.* **214**, 1992-1930.

Willert, C. E. and Gharib, M. (1991). Digital particle image velocimetry. *Exp. Fluids* **10** (4), 181-193.

Wilson, S. C., Pierce, G. J., Higgins, C. M. and Armstrong, M. J. (2002). Diet of the harbour seals *Phoca vitulina* of Dundrum Bay, north-east Ireland. *J. Mar. Biol. Assoc. U.K.*. **82** (6), 1009-1018.

Woolsey, T. A. and Van der Loos, H. (1970). The structural organization of layer IV in the somatosensory region (SI) of mouse cerebral cortex. The description of a cortical field composed of discrete cytoarchitectonic units. *Brain Res.* **17**, 205-42.

Figures

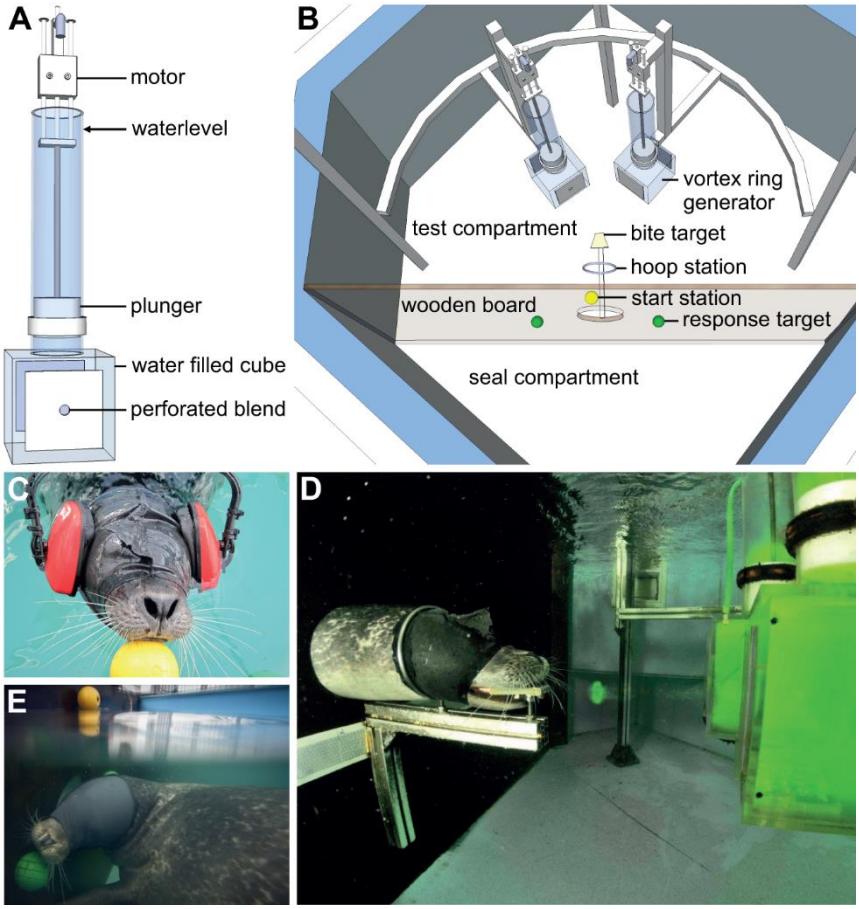

Fig. 1: **Experimental setup and psychophysical procedure. A** Schematic drawing of one vortex ring generator (VRG). A remote controlled motor pushed down the plunger within the tube and expelled water through the aperture of the blend. **B** Experimental setup, viewed from above, with a wooden board separating the pool into a seal's compartment and a test compartment in which two VRGs were mounted on a semi-circular horizontal profile. The animal's underwater stationing consisted of a hoop station and a bite target (distance to the apertures of the VRGs: 30 cm). A start station (yellow plastic sphere) and two underwater response targets (green plastic spheres) were fixed to the wooden board. Two timber planks that were positioned across the pool served as working platforms. These planks, the wiring of the motors to the technical equipment (stored in an external cabinet close to the pool), and the remote are not shown. **C** A harbour seal stationing at the start station prior to the trial. It is supplied with a visually opaque elastic mask and headphones transmitting pink noise. **D** A blindfolded harbour seal stationing on a bite target in the test compartment. The vortex ring,

generated by the left VRG, is travelling towards the protruding mystacial vibrissae. The water within the cubes of the VRGs was stained with uranine. The reflective band used for precise orientation of the generators can be seen attached to the wooden board, on either side of the underwater station (Photo credit: Eckhard Krumpholz). **E** A harbour seal responding correctly on the left response target by touching it with its snout (Photo credit: Fabian Fiechter).

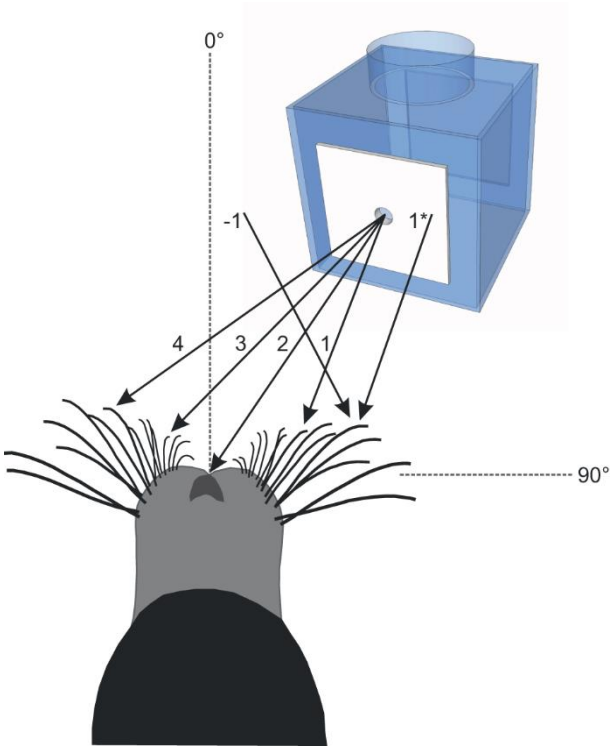

Fig. 2: **Six possible travel paths of a vortex ring in experiment 3 generated by the right VRG**. Travel path 1* and -1 are the travel paths used in the control experiments. Travel paths 1 and 2 were also used in experiment 1 and 2, respectively.

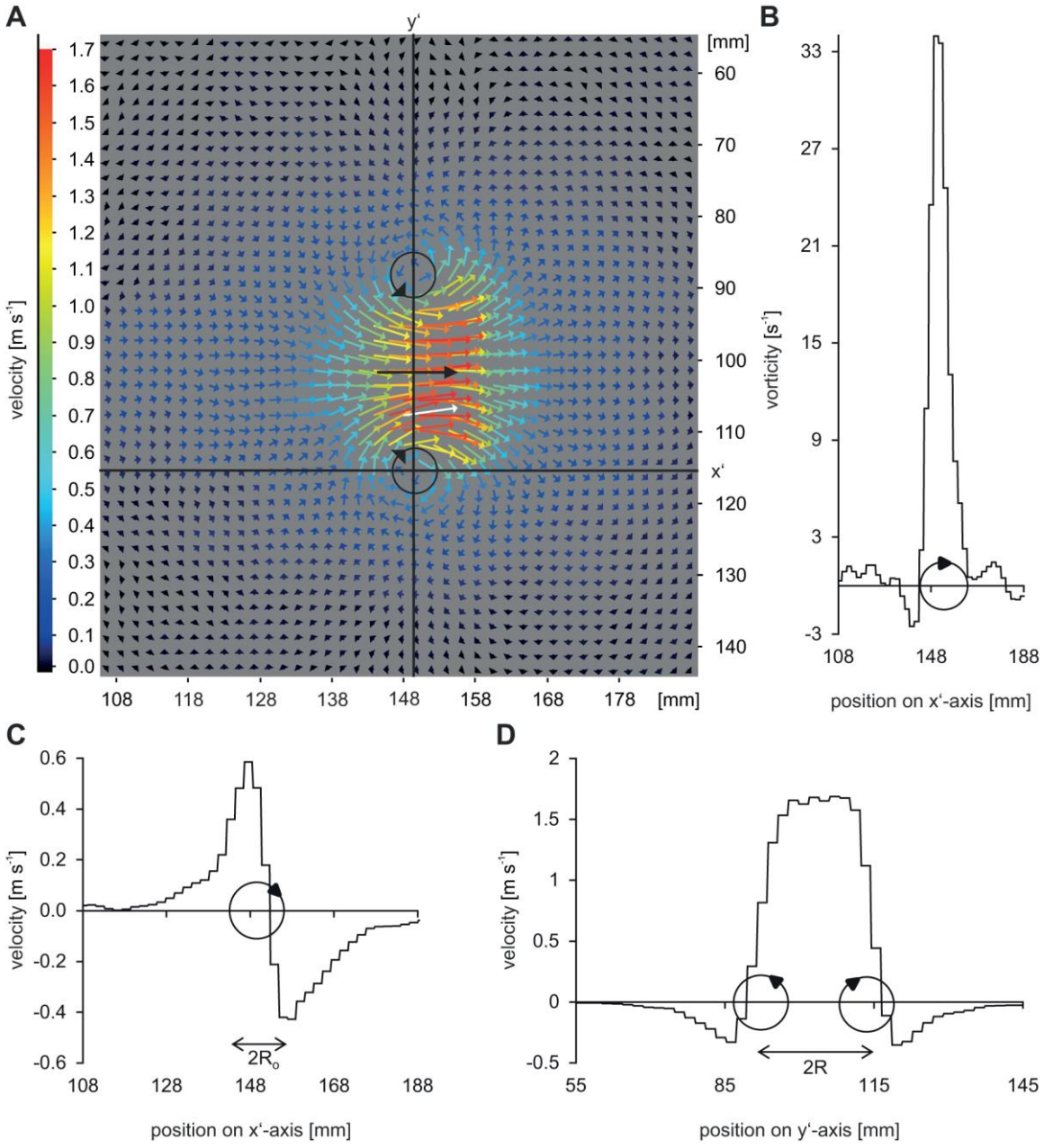

Fig. 3: **Results of the vortex ring analysis. A** Water velocity vector graph of vortex ring S2 150 mm from the aperture of the blend. The colour code and vector length indicate the velocity. The white vector depicts the absolute maximum velocity within the jet of the vortex ring. Dark blue and black represent the lowest velocities. The black arrow in the centre shows the travel direction of the vortex ring. Vortex cores of the counter-rotating vortices are indicated as black circles. Arrowheads show the rotational direction. **B-D** Profiles of the vortex ring according to the framework established by Spedding (1987) and Müller et al. (1997). All profiles were taken through the centres of the counter-rotating vortices. **B** Distribution of the vorticity along the x'-axis. **C** Velocity profile plotted along the x'-axis. R_o = vortex core radius. **D** Distribution of the velocity along the y'-axis. R = vortex ring radius.

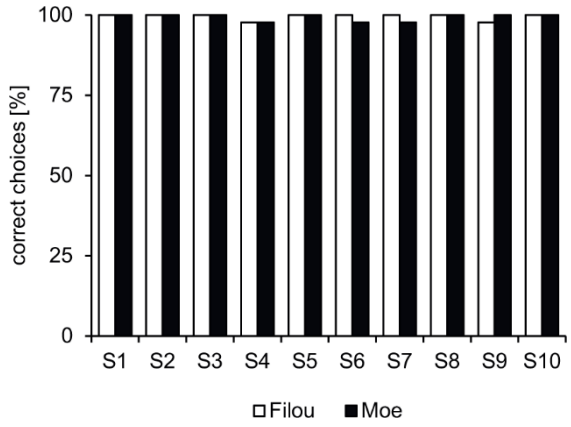

Fig. 4: **Performance of Filou (white bars) and Moe (black bars) in experiment 1 for 10 stimuli (S1 – S10) pooled over three sessions** (each bar represents 45 trials). All stimuli were detected with a highly significant performance (χ^2-test, P<0.001, N=45).

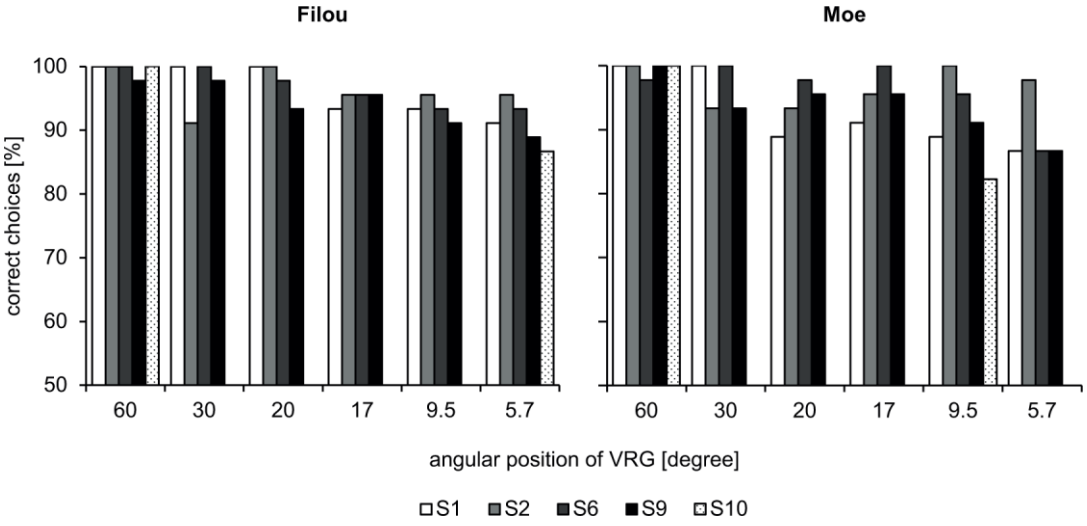

Fig. 5: **Ability of Filou (left) and Moe (right) to determine the side where a vortex ring came from.** Five stimuli (S1, S2, S6, S9, and S10) were presented. Angular positions of the VRGs varied between 5.7 and 60°. Each bar represents the result of 45 trials. The correct side was detected for each vortex ring (χ^2-test, P<0.001, N=45).

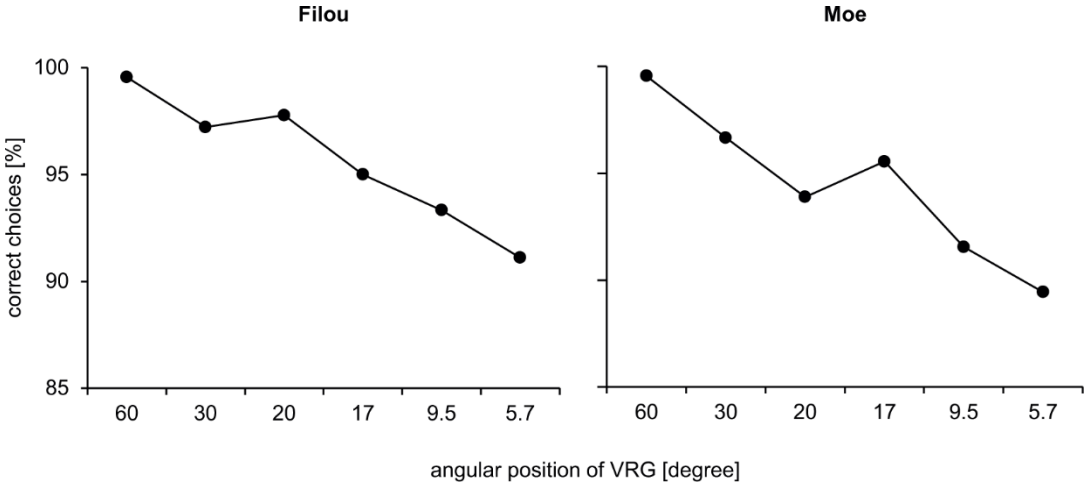

Fig. 6: **Performance of Filou (left) and Moe (right) for the determination of the MHPA.** These data show the mean performance for all stimuli (S1, S2, S6, S9, and S10) as a function of the angular position of the VRGs. Each data point represents the pooled result of 225 or 180 trials depending on the number of stimuli presented per position (Filou: 60° and 5.7°: 225 trials, 30°, 20°, 17°, and 9.5°: 180 trials; Moe: 60° and 9.5°: 225 trials, 30°, 20°, 17°, and 5.7°: 180 trials). All data points are highly significant (χ^2-test, P<0.001).

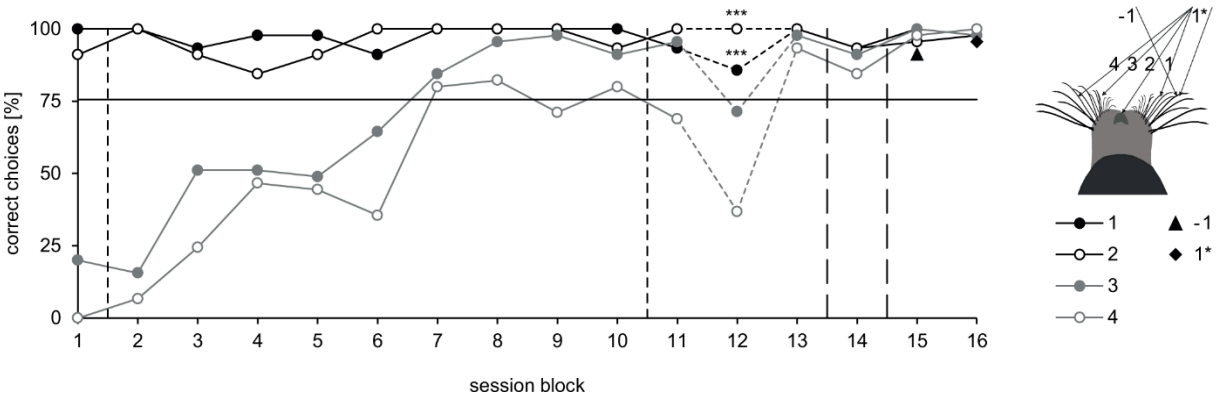

Fig. 7: **Filou's performance in detecting the travel direction of a single vortex ring (S9) along four different travel paths plotted against the session blocks**. Each session block consisted of 45 trials per data point except for session block 12 in which only 36 trials were conducted due to moulting. The horizontal line indicates the level of significance (χ^2-test, P<0.001, *N*=45) for all data points (excluding session block 12: the three asterisks indicate highly significant performance). In the first session block, Filou performed the task blindfolded to test his spontaneous performance in the new task. Session blocks 2 to 10 are learning sessions in which Filou was not blindfolded. The blindfold was applied again thereafter for all following session blocks. Session block 14 is the transfer session in which new stimuli (S1, S2, S9, and S10) were presented. The two control sessions with new travel paths are shown in session block 15 (triangle: performance for travel path -1) and block 16 (diamond: performance for travel path 1*).

Tab. 1: **Motor parameters and vortex ring properties of 10 vortex rings (S1 – S10) used in the psychophysical experiments.** The motor parameters velocity (0.5 m s^{-1}) and deceleration (10 m s^{-2}) were constant for all stimuli. The vortex ring size is calculated by averaging 10 data points per image along the travel path within the area of 200 mm to 315 mm from the aperture of the blend. The maximum velocity is averaged from the 10 highest velocity vectors per image within the area of 100 mm to 315 mm from the aperture, and calculated by linear regression for two positions from the aperture, 23 cm and 34 cm. Acceleration and stimulus duration are calculated for the area of vibrissal stimulation.

	motor parameters		vortex ring properties						
vortex ring	amplitude [mm]	acceleration [m s^{-2}]	mean size ± s.d. [mm]	max. velocity [m s^{-1}] 23 cm	max. velocity [m s^{-1}] 34 cm	travel velocity [m s^{-1}] 23 cm	travel velocity [m s^{-1}] 34 cm	acceleration [m s^{-2}] 23-34 cm	stimulus duration [s] 23-34 cm
S1	3.0	10	89.89 ± 3.31	2.108	1.800	1.073	0.903	-1.574	0.108
S2	2.0	10	68.95 ± 1.58	1.397	1.111	0.649	0.494	-0.858	0.180
S3	1.5	10	59.49 ± 0.96	0.910	0.701	0.424	0.299	-0.447	0.276
S4	1.0	10	31.29 ± 1.71	0.224	0.158	0.144	0.115	-0.036	0.807
S5	3.0	0.5	87.64 ± 3.35	2.069	1.684	1.057	0.897	-1.457	0.109
S6	2.0	0.5	65.93 ± 0.85	0.979	0.561	0.444	0.235	-0.785	0.262
S7	1.5	0.5	51.11 ± 1.36	0.763	0.554	0.356	0.246	-0.332	0.329
S8	3.0	0.2	65.31 ± 1.36	0.817	0.630	0.378	0.287	-0.296	0.309
S9	2.0	0.2	54.14 ± 1.90	0.666	0.424	0.301	0.195	-0.270	0.389
S10	1.5	0.2	45.78 ± 1.11	0.538	0.263	0.262	0.166	-0.213	0.447